

Charalabos C. Doumanidis

Sampled weighted attraction control of distributed thermal scan welding

*Kybernetika*, Vol. 35 (1999), No. 1, [117]--132

Persistent URL: <http://dml.cz/dmlcz/135272>

## Terms of use:

© Institute of Information Theory and Automation AS CR, 1999

Institute of Mathematics of the Academy of Sciences of the Czech Republic provides access to digitized documents strictly for personal use. Each copy of any part of this document must contain these

*Terms of use.*



This paper has been digitized, optimized for electronic delivery and stamped with digital signature within the project *DML-CZ: The Czech Digital Mathematics Library*  
<http://project.dml.cz>

## SAMPLED WEIGHTED ATTRACTION CONTROL OF DISTRIBUTED THERMAL SCAN WELDING

CHARALABOS C. DOUMANIDIS<sup>1</sup>

This article addresses the problem of distributed-parameter control for a class of infinite-dimensional manufacturing processes with scanned thermal actuation, such as scan welding. This new process is implemented on a robotic GTAW laboratory setup with infrared pyrometry, and simulated by a flexible numerical computation program. An analytical linearized model, based on convolution of Green's fields, is expressed in multivariable state-space form, with its time-variant parameters identified in-process. A robust controller design compensates for model uncertainty, and a sampled weighted attraction method is introduced for heat source guidance based on real-time thermal optimization of the heat input distribution. The distributed thermal regulation strategy with infrared feedback is validated both computationally and experimentally in scan welding tests.

### 1. INTRODUCTION

Since the early days of Hephaistos, the smith of the Olympian gods, thermal processing of materials has been consistently at the heart of virtually every industrial fabrication method, besides high-tech weaponry. In the automotive industry, for example, the molds of the car body are sculpted by automated deposition of their material guided by innovative thermal Rapid Prototyping techniques, rather than by manual forging, to keep up with the changing fashions in aesthetics and aerodynamics. In the electronics and computer industry, the need for faster and more powerful microprocessor chips is satisfied by sophisticated thermal processing of thin semiconductor film structures of high purity for implementation of complex circuitry. In telecommunications, the constantly increasing use of fiber optics has been made possible through the stringent quality specifications of optical fibers produced in thermal drawing furnaces. Last, in biomedical technology, the fabrication of prosthetic or replacement aids for injured or amputated organs, such as total hip replacement, relies heavily on special thermal production and processing of new alloys and composites, to ensure the required strength, durability and biocompatibility. In all these multifaceted applications, the quality of the thermal product, described by its geometric morphology, material structure and mechanical proper-

---

<sup>1</sup>This research was supported by NSF Grant DMI-9553038.

ties distribution, is determined by the dynamic, spatially distributed temperature field generated in the part during the process. Despite the clear infinite-dimensional nature of the thermal dynamics, however, real-time control of such manufacturing methods has invariably been addressed in the context of finite-dimensional regulation of a few localized thermal product features. In the welding literature, for example, the weld bead dimensions [1], the heat affected zone size and cooling rate [5], as well as certain residual stress and thermal deformation attributes [9], are controlled through the heat source power and speed, and possibly the rate of material feeding. The limited number of such independently manipulable process conditions, i. e. the variables of welding torch or heat treatment oven, which can serve as control inputs for the regulation of commensurate thermal outputs, is the reason for this lumped-parameter approach. However, the recent advent of more flexible thermal actuators, such as Laser and electron beams, together with sensors based on optical or infrared cameras and radiographic or ultrasonic imaging systems, enable new approaches to the distributed-parameter thermal control problem. In this direction, infinite-dimensional systems theory [3, 10, 11] has inspired the redesign of classical localized, serial thermal processing methods into novel parallel techniques with distributed actuation and sensing. The recently patented Scan Welding process is such a paradigm [4]. Rather than the localized heating of a sequentially-moving, conventional welding torch, the scan welding heat source sweeps rapidly the entire accessible surface of the weld, and its power is dynamically varied along its motion to provide a flexible continuous heat input distribution. This distributed action of the scanned Laser beam or robotically driven torch on the external surface is modulated to generate a specified temperature field in the part volume, yielding the desired geometric, structural and mechanical quality of the material. Manipulation of this scanned heat influx on the part boundary is based on real-time measurement and feedback of its external temperature distribution, e. g. by an infrared pyrometry sensor. The design and implementation of a closed-loop thermal control strategy for such a distributed scan welding process is the objective of this article.

## 2. EXPERIMENTAL STATION AND NUMERICAL SIMULATION

In the laboratory setup for general thermal processing and scan welding tests, the heat source is reciprocated on an in-process modulated trajectory, at a frequency considerably faster than the thermal dynamics of the part, by an articulated 6 d.o.f. process robot. The scanned path consists of straight motion at constant velocity between dynamically defined points, with parabolic blends of constant acceleration/deceleration between the linear segments. The source is a Gas Tungsten Arc Welding (GTAW) torch, powered by a multiprocess power supply transformer. In the experiments, the arc length is 3 mm, the voltage 15 V and the flow rate of the shielding gas (Ar-2%O<sub>2</sub>) is 0.6 lt/s. The tests consist of bead-on-plate scan welding of stainless steel coupons (304), measuring 30 × 24 × 3 mm. The robot trajectory and GTAW torch power are manipulated in real time by the control computer of the system, using feedback of thermal measurements on the top weld surface by an infrared pyrometric camera. The infrared sensor consist of a 2-D electromechanical scanner

and a liquid nitrogen-cooled HgCdTe detector element, sensitive in the 8–12 mm wave length range. This provides a spatial resolution of about 0.12 mm on the part surface, and a temperature sensitivity of +2 K in a 1000 K range. The infrared images, besides providing real-time temperature feedback at a user-defined emissivity to the system computer through a frame grabber, are also stored in composite video format for off-line analysis by special thermal image processing software.

Besides laboratory experimentation, the distributed-parameter thermal controller for scan welding will be tested computationally on an off-line flexible numerical simulation of the temperature and material structure field developed in the weld [4]. This dynamic model of scan welding is based on integration of a finite-difference formulation of heat transfer by solid conduction, with an embedded liquid flow model in molten areas of the part (Figure 2.1):

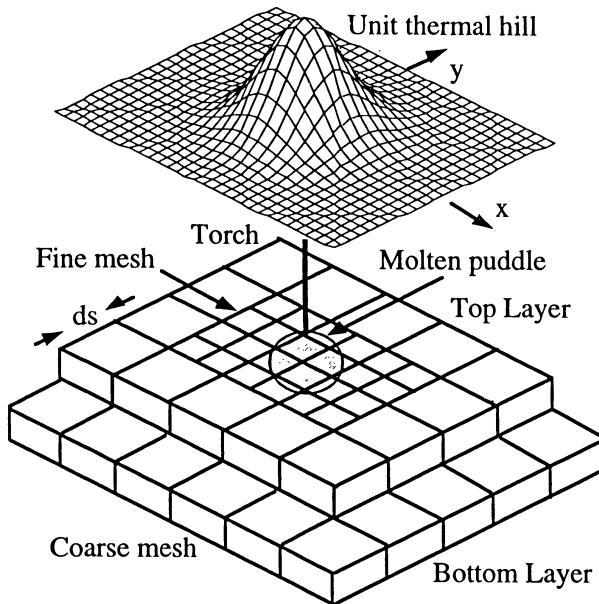


Fig. 2.1. Numerical simulation of scan welding with unit thermal perturbation hill.

$$\begin{aligned}
 T(x, y, z; t + \delta t) = & T(x, y, z; t) + \frac{\alpha dt}{ds^2} \sum_{i=1}^6 \gamma_i T_i(x \pm ds, y \pm ds, z \pm ds; t) \\
 & - T(x, y, z; t) + \frac{2\alpha dt}{\lambda ds} (Q(x, y, 0; t) - Q_e(x, y, 0; t))
 \end{aligned}
 \tag{2.1}$$

where  $T$  is the temperature at location  $(x, y, z)$  and time  $t$ ,  $T_i$  the temperatures at its six surrounding locations in the three dimensions at distance  $ds$ , and  $dt$  the integration time step.  $\alpha$  is the thermal diffusivity and  $\lambda$  the conductivity of the solid

material, and  $\gamma_i$  the directional equivalent conduction factors in the molten puddle in the respective dimensions ( $\gamma_i = 1$  for the solid, [4]). The heat input distribution  $Q$  and surface loss  $Q_e$  term, which includes conductive, convective and radiative heat flow to the environment, are present in (2.1) only for points on the external part boundary. The numerical model provides for a wide variety of orthogonal and cylindrical object geometries, covered by multiple meshes of nodes with a coarser spacing in the heat affected zone and a finer spatial resolution near the molten puddle. The meshes can be configured to be stationary in the prototype or follow the source motion, and emulate deposition or removal of filler material by respective activation or deactivation of nodes on superposed layers. The simulation accounts for arbitrary heat input distributions on the part surface by one or multiple heat sources, as well as temperature-dependent material properties and latent transformation effects (i. e. fusion and solidification). The simulation code provides the full dynamic thermal history of the process in the form of 3-D temperature and material phase maps, 2-D thermal hills and isotherm contours, as well as the time responses of various individual thermal features.

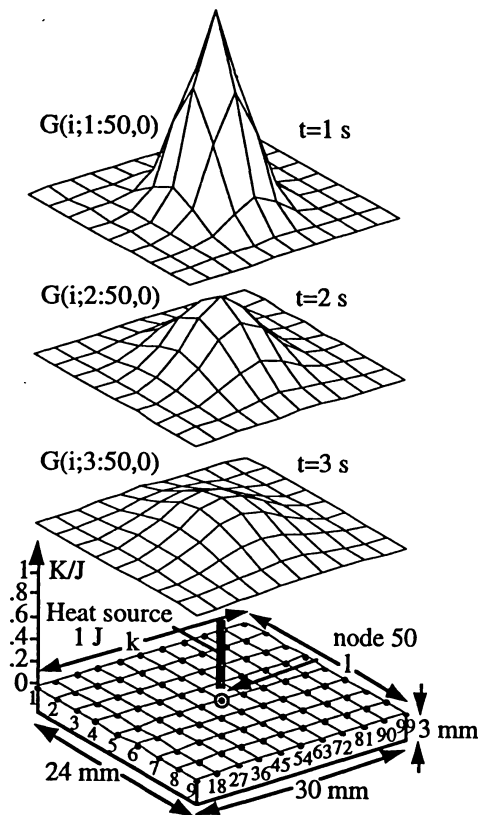


Fig. 2.2. Orthogonal mesh for temperature outputs and heat inputs for the linear MIMO model, and Green's field  $G(i; t : 50, 0)$  at  $t = 1, 2, 3$  s.

### 3. MULTIVARIABLE THERMAL MODELING

In parallel to off-line validation of an infinite-dimensional thermal control scheme on the numerical simulation above, its design must be established on the insights provided by a simpler analytical thermal description. Such a computationally efficient, real-time thermal model for the distributed-parameter scan welding process can be formulated as a finite-dimensional, multivariable expression of the temperature output with respect to the heat input distribution at discrete, representative mesh points of the weld. Figure 2.2 defines such a low-order model for scan welded orthogonal sheets, in which the dynamic, lumped temperature states  $T(i; t)$ ,  $i = 1, \dots, n$  and heat inputs  $Q(j; t)$ ,  $j = 1, \dots, m$  are described by the respective vectors of local values at the nodes of an orthogonal mesh of size  $k = 11$ ,  $l = 9$  ( $n = m = k \cdot l = 99$ ). The square mesh element size  $Ds = 3$  mm is chosen by compromise between spatial resolution and computational conciseness of the model. In this arrangement, a linearized analytical formulation of the process dynamics is based on the assumption of linear transient solid conduction in a uniform and isotropic material, with temperature-invariant thermal properties and no latent transformation effects. Linear heat losses from the free weld surface and a Gaussian power density distribution of the heat source is also assumed. The dynamic description of the output vector  $T$  on the input vector  $Q$  is established on the concept of the Green's matrix  $G(i; t : j; t)$ , the elements of which express the transient temperature  $T$  at node  $i$  and time  $t$ , generated by an impulsive unit heat input  $Q$  at node  $j$  and time  $t$  [2]. The Green's parameters can be expressed analytically for a plate as a series of thermal images:

$$G(i; t : j; \tau) = \sum_{h=1}^n \frac{\eta}{16\pi\sigma^2\rho c[\pi\alpha(t-\tau)]^{\frac{3}{2}}} \exp\left(-\frac{(x(i)-x(h))^2+(y(i)-y(h))^2}{4\gamma\alpha(t-\tau)} - \frac{2\alpha(t-\tau)}{\rho c H} - \frac{(x(h)-x(j))^2+(y(h)-y(j))^2}{2\sigma^2}\right) \quad (3.1)$$

where  $x(i)$ ,  $y(i)$  are the coordinates of the temperature output node  $i$ ,  $x(j)$ ,  $y(j)$  those of the heat input node  $j$ , and  $x(h) = Ds \cdot \text{int}(h-1, l)$ ,  $y(h) = Ds \cdot \text{mod}(h-1, l)$  of node  $h$ . The material parameter  $\rho$  is the density,  $c$  the heat capacity and  $\gamma$  the equivalent conductivity factor in the melt ( $\gamma = 1$  in the solid region as in (2.1)).  $H$  is the plate thickness,  $\alpha$  the equivalent linearized heat transfer coefficient on the weld surface, and  $\eta$ ,  $\sigma$  the efficiency and distribution radius of the power density distribution of the source. Alternatively to (3.1), estimates of the Green's matrix elements can be obtained by the numerical simulation above (2.1), as the dynamic temperature values  $T$  obtained after a unit heat input perturbation  $Q$ . Figure 2.2 illustrates the distribution of Green's parameters  $G(i; t : 50; 0)$  on the coupon of Figure 2.2, by a unit heat input at the center node, at several elapsed times after the torch action. Thus, the linearized temperature hill  $T$  can be derived by convolution of this dynamic field with the thermal power input  $Q$  throughout its trajectory on the part during the process:

$$\underline{T}(i; t) = \underline{T}(i; 0) + \int_0^t G(i; t : j; \tau) \cdot \underline{Q}(j; \tau) d\tau \quad (3.2)$$

Figure 2.2 clearly shows that solid conduction results in a decaying transient, localized, radially symmetric temperature hill in the vicinity of the heat input, with almost no effect at remote points. This indicates that the Green's matrix  $G(i; t : j; t)$  contains only a small number (at most  $n - l(l - 1)/2$ ) of nontrivial elements  $G(r, d)$ , for limited ranges of radial distance

$$r = \sqrt{[x(i) - x(j)]^2 + [y(i) - y(j)]^2}$$

and time delay  $d = t - \tau$ . In addition, if heat losses from the weld edges are equivalent to the internal conductive heat flux, as for example when the coupon of Figure 2.2 is part of a larger plate, then the matrix  $G$  has a sparse, banded, diagonally uniform, symmetric structure (when  $n = m$ ), with its subdiagonals containing identical elements. This special structure of  $G$  greatly facilitates real-time efficient computation of the superposition (3.2), and is graphically depicted in Figure 3.1.

However, scan welding involves nonlinearities and time variations of the heat transfer mechanisms, such as radiation effects, thermal drift of temperature-dependent material properties, structural transformations with latent thermal phenomena (fusion and solidification), and alteration of torch characteristics. These effects yield variable dynamic parameters in the linearized model (3.2), during the transients and disturbances of the process from its nominal conditions. Thus, the initial off-line estimates of the time-variant constitutive elements of the Green's matrix  $G(i; t : j; t)$ , obtained analytically (3.1) or numerically (2.1) as explained, must be updated in-process by measurements  $T$  on the part surface. Such real-time identification of the Green's parameters is based on incremental deconvolution of (3.2) in discrete time steps  $Dt$  [1]:

$$\begin{aligned} \underline{T}(i; t) - \underline{T}(i; \tau) - \int_0^t G(i; t - Dt : j; \tau) \cdot \underline{Q}(j; \tau) d\tau & \quad (3.3) \\ = [G(i; t : j; \tau) - G(i; t - Dt : j; \tau)] \int_0^t \underline{Q}(j; \tau) d\tau. \end{aligned}$$

Thus, the numerically significant parameters in  $G(i; t : j; \tau)$  can be determined by commensurate linearly independent equations for an equal number of nodes  $i$ , selected out of the  $n$  relations in (3.3). Multiple solutions for various selections of nodes  $i$  can be averaged to reduce estimation errors. Equation (3.2) expresses the linearized thermal model in vectorized input-output integral form. An equivalent alternative description in state-space differential formulation can also be derived to facilitate the design of thermal controllers by familiar pole placement of linear quadratic techniques:

$$\dot{\underline{T}}(i; t) = A(i, h; t) \cdot T(h; t) + B(i, j; t) \cdot Q(j; t) \quad (3.4)$$

where the temperature state vector  $\underline{T} = \underline{T} - \underline{T}_d$  and the heat input vector  $\underline{Q} = \underline{Q} - \underline{Q}_d$  are measured relative to a nominal setpoint of operating conditions  $(\underline{T}_d, \underline{Q}_d)$ . The time-varying  $n \times n$  state matrix  $A(i, h; t)$  and the  $n \times m$  input matrix  $B(i, j; t)$  express the thermal rate of change at node  $i$  because of the current temperature  $T$  at node  $h$  or the heat input  $Q$  at node  $h$  respectively. Under the previous assumptions of linear

solid conduction, these matrices can also be determined by analytical expressions derived from equation (3.1), since they are related to the Green's matrix  $G$ :

$$A(i, h; t) = \dot{G}(i; t : j; \tau) \cdot G^{-1}(j; t : h; \tau), \quad B(i, j; t) = \dot{G}(i; t : j; t). \quad (3.5)$$

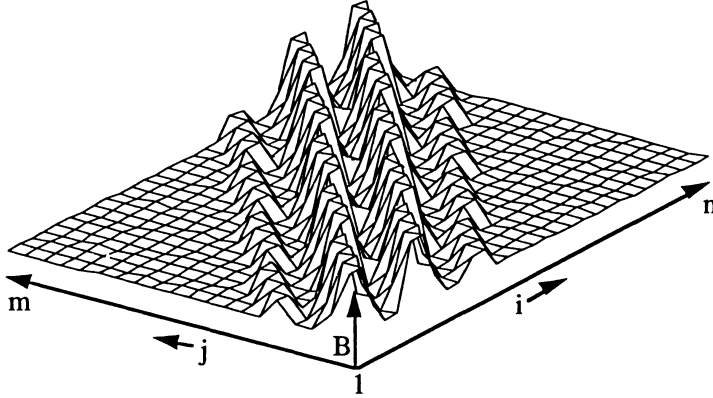


Fig. 3.1. Graphical rendering of the structure of matrices  $A, B, K, \hat{A} = A + BK$ .

By arguments similar to those for the Green's matrix  $G$ , the system matrices  $A$  and  $B$  are also composed by a small number of independent elements  $A(r, d)$  and  $B(r, d)$ . Moreover, equation (3.5) preserve the uniform diagonal bands and the symmetry of the state matrix  $A$  and input matrix  $B$  (if  $n = m$ ), which thus display a form similar to  $G$  (Figure 3.1). Again, this structure enables real-time eigenstructure analysis of the linearized model description  $\{A, B\}$ , through special sparse matrix techniques based on order reduction [6]. However, the nonlinearities of the scan welding process yield state-dependent dynamic parameters in the linear model of (3.4), as expected. Thus in the neighborhood of the nominal conditions  $(\underline{T}_d, \underline{Q}_d)$  the nonlinear thermal system can be linearized to a linear, time-variant (LTV) formulation, with the system matrices  $\{A, B\}$  consisting of a stationary and a non-stationary (time-dependent) component:

$$A(i, h; t) = A_0(i, h) + DA(i, h; t), \quad B(i, j; t) = B_0(i, j) + DB(i, j; t) \quad (3.6)$$

where  $A_0, B_0$  are their constant values at the operating point and  $DA(t), DB(t)$  their uncertain parts. The latter depend on time-varying process parameters, such as torch efficiency and distribution, the thermal material properties and the heat loss parameters to the environment. After the determination of the certain components  $A_0, B_0$  at the nominal setpoint as above, the uncertain parts

$$DA(t) = A(t) - A_0, \quad DB(t) = B(t) - B_0$$

can be evaluated similarly under process conditions other than the nominal.

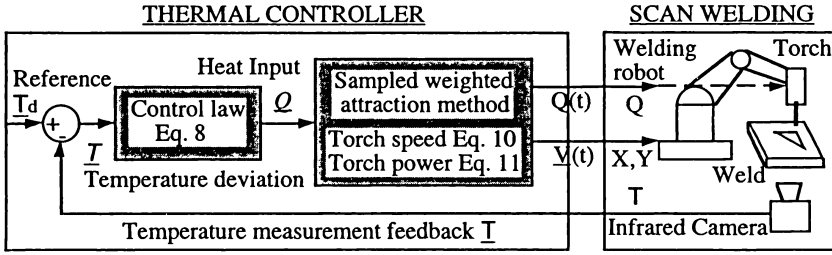


Fig. 3.2. Block diagram of closed-loop thermal control system for scan welding.

#### 4. ROBUST CONTROL AND TORCH GUIDANCE

The time variation of the scan welding description in (3.4) mandates the robustness of the thermal control system to be designed, to the structured uncertainty of the model parameters. Such a multivariable controller employs feedback of the temperature measurement  $T$  deviations from the nominal field  $T_d$ , to modulate the thermal distribution  $Q$  on the weld surface with respect to the reference heat input  $Q_d$  (Figure 3.2):

$$\underline{Q}(j;t) - \underline{Q}_d(j) = K(j,h) \cdot [\underline{T}(h;t) - \underline{T}_d(h)] \quad \text{i.e.} \quad \underline{Q}(j;t) = K(j,h) \cdot \underline{T}(h;t) \quad (4.1)$$

where the  $n \times m$  control gain matrix  $K = K_0 + DK$  consists of a standard part  $K_0$ , designed on the basis of the certain model description  $\{A_0, B_0\}$ , and an additional part  $DK$  to handle the uncertain process component  $\{DA(t), DB(t)\}$ . The design of this robust MIMO controller is elaborated in the Appendix. Thus, by combining the control law of (4.1) to the process model of (3.4), the thermal dynamics of the closed-loop scan welding system can be described as:

$$\dot{\underline{T}}(i;t) = [A(i,h;t) + B(i,j;t) \cdot K(j,h)] \cdot \underline{T}(h;t) = \hat{A}(i,h;t) \cdot \underline{T}(h;t) \quad (4.2)$$

where  $\hat{A} = A + BK$  is the state matrix of the thermal feedback system. Its dynamics can be properly designated by linear quadratic methods or pole placement [9] of the eigenstructure of matrix  $\hat{A}$ . As it can be concluded in the Appendix (Eq.18), the controller gain matrix  $K$ , and thus the system state matrix  $\hat{A}$ , have also a sparse, uniformly diagonal banded, symmetric structure (if  $n = m$ ) similar to the model matrices  $A$  and  $B$  (Figure 3.1). This indicates that the heat input  $Q(j;t)$  at a node  $j$  in (4.1) is actually determined by the temperatures  $T(h;t)$  of a few adjacent nodes  $h$ , corresponding to the numerically significant gains of the controller  $K(j,h)$ . Thus the control law (4.1) obtains the node heat inputs  $Q(j;t)$  by a computationally efficient spatial weighting of the measured neighboring node temperatures  $T(h;t)$ . In Figure 3.2, for a stable design of the feedback system ( $\hat{A}$ ), this modulation of the heat input distribution  $Q$  results in a temperature field  $T$  following asymptotically the desired thermal reference  $T_d$ , despite the process uncertainties and disturbances. The manipulated heat distribution  $Q$  could be directly

implemented by high-bandwidth heat sources, such as Laser and electron beams, by fast raster-scanning of the weld surface (similar to a CRT monitor), i.e. by dynamically adjusting the scanning beam intensity to provide the proper heat input  $Q(j;t)$  to each element (pixel)  $j$  of the orthogonal mesh in Figure 2.2. However, for slowly moving sources, such as the robotic GTAW torch, the distribution  $Q$  can be best approximated by vector-scanning of the source on a dynamic trajectory  $X(t), Y(t)$  (similar to an oscilloscope screen). The torch motion is directed towards the location of highest thermal demand, i.e. the maximum of the  $Q$ -surface (Figure 4.1), with simultaneous adjustment of its power  $Q(t)$ . Thus, the guidance and modulation of the heat source in the scan welding thermal system is posed as a distributed-parameter dynamic optimization problem, i.e. real-time tracking of the locus of the moving maximum of the  $Q$ -surface, linearly interpolated to the control values  $Q(j;t)$  (4.1). In principle, a standard steepest-ascent method could be used for this purpose, driving the torch along the gradient of the  $Q$ -surface at a proportionate velocity  $\underline{V}(t) = c \cdot \nabla Q(j;t)$ . However, this technique is hampered by practical difficulties, since it requires exact modeling and extensive sensing in the vicinity of the heat source, which is problematic because of the welding arc effects. In addition, computation of derivatives for the gradient-based method is untrustworthy because of its sensitivity to thermal noise of the temperature data  $T$ . Moreover, since the slope of the thermal distribution near the source does not convey information on its full landscape, this technique tends to lead the torch to the nearest local maximum of the  $Q$ -surface and ignore its remote peaks (Figure 4.1). This guidance strategy

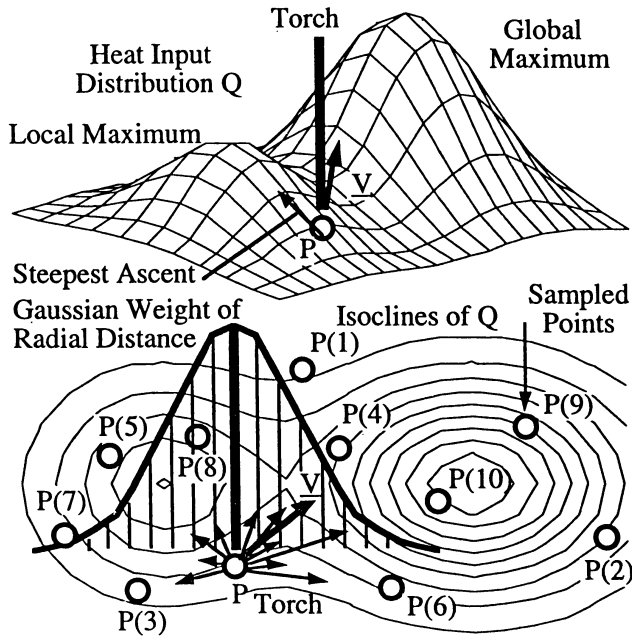


Fig. 4.1. Guidance of heat source motion by sampled weighted attraction.

favors elimination of local heat deficiencies before passing the heat source to the region of the global maximum of the thermal deviation, thus showing a reluctance to fast torch motion and degrading the welding performance. For scan welding of large parts with non-uniform heat demands and strict regulation specifications, a trajectory control scheme must be based on comprehensive thermal data from the entire part surface, beyond the local conditions near the torch.

Such a global thermal optimization technique, the Sampled Weighted Attraction method is introduced, based on in-process random sampling of the entire distribution surface (Figure 4.1). At a fixed number  $N$  of randomly located positions  $\underline{P}(h;t)$ ,  $h = 1, \dots, N$  on the part surface ( $N$  depending on the desired thermal resolution), the actual spot temperatures  $T(h;t)$  are measured and the necessary heat inputs  $Q(h;t)$  are computed by (4.1). Then the torch velocity  $V(t)$  is defined as consisting of  $N$  individual components, directed from the torch location  $P(t)$  to each position  $P(h;t)$ , with magnitude proportional to the respective heat input  $Q(h;t)$ , and weighted according to the distance of each point from the source by a Gaussian distribution:

$$\underline{V}(t) = \sum_{h=1}^N C_V Q(h;t) [\underline{P}(h;t) - \underline{P}(t)] \exp\left(-\frac{|\underline{P}(h;t) - \underline{P}(t)|^2}{2s^2}\right) \quad (4.3)$$

where  $|\cdot|$  is the Euclidean distance norm,  $C_V$  the velocity gain and  $s$  the distribution radius of the Gaussian weighting distribution. Similarly, the power  $Q(t)$  of the heat source is also defined as:

$$Q(t) = \sum_{h=1}^N C_Q Q(h;t) \exp\left(-\frac{|\underline{P}(h;t) - \underline{P}(t)|^2}{2s^2}\right) \quad (4.4)$$

where  $C_Q$  is the power gain. Next, every sampling period  $Dt$  the oldest sample location  $P(h;t)$  among the  $N$  points is replaced by a new randomly selected position on the weld surface, and the procedure is continuously repeated and gradually guides the heat source  $P(t)$  to the global maximum of the heat input surface  $Q$ . The number of sampling locations  $N$  entering the calculations of the weighted attraction Eqs. (4.3) and (4.4) influences the speed (faster for lower  $N$ ) and smoothness (better for higher  $N$ ) of the torch trajectory. Also in random sampling of new locations, instead of the assumed uniform probability distribution, a more directed sampling can be implemented if a variable Boltzmann (axisymmetric radially exponential) probability profile is adopted. This can be centered at the thermally weighted centroid of the sampled  $N$  points and with a distribution radius commensurate to their weighted standard deviation. This adjustable probability distribution can give this method simulated annealing features [8]: In the presence of several local peaks of the  $Q$ -surface, the sampled  $N$  points are scattered on the weld surface and their large standard deviation from their centroid leads to sampling of new points in a broader region, thus expanding the search for the global optimum. On the contrary, when this global maximum of  $Q$  is approached by the source, the centroid of the sampled points is attracted to its vicinity, leading to a small deviation and thus a localized sampling, contributing to faster convergence and tracking of the optimum.

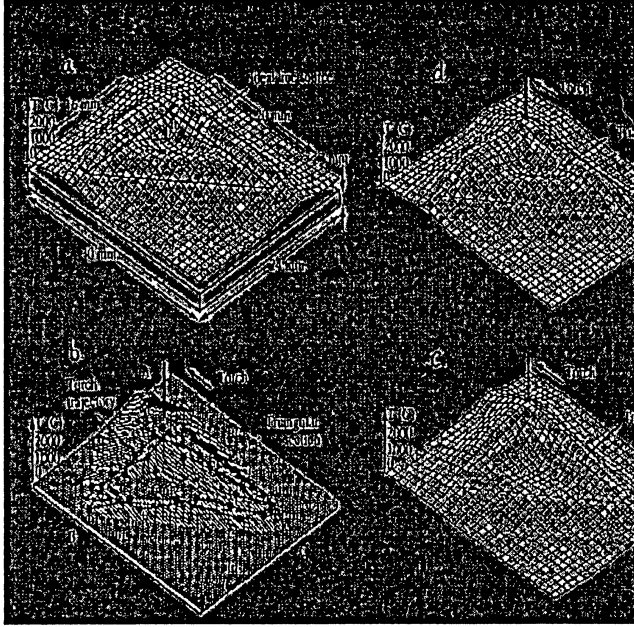


**Fig. 4.2.** Closed-loop scan welding of a triangular flange section at steady state ( $t = 20$  s):  
 a. Reference temp. hill  $T_d$  by line source (simulated), b. Measured temp. hill  $T$  by IR camera ( $Dt = 1$  s), c. Simulated temp. hill  $T$  ( $Dt = 1$  s), d. Simulated temp. hill  $T$  ( $Dt = 1$  s).

## 5. EXPERIMENTAL AND COMPUTATIONAL TESTING

The performance of this distributed-parameter control methodology is assessed in an elementary scan welding operation, both by computational simulation, where the numerical model (2.1) replaces the process hardware, and by experimental testing on the laboratory setup. The stainless steel plate of Figure 2.2 is scan welded along a composite triangular flange pattern. Figure 4.2a shows the necessary nominal temperature field  $T_d$  for this operation, generated by an ideal three-segment ( $\Delta$ ) uniform line heat source  $Q_d = 50$  kW/m, along the processed edges through computer simulation. Alternatively, this nominal thermal hill may be developed directly in the laboratory during a satisfactory off-line reference test, and recorded by the infrared pyrometer in order to be subsequently reproduced by the thermal feedback control system. In closed-loop operation, the temperature measurements  $\underline{T}(h; t)$  at the grid nodes determine the heat inputs  $\underline{Q}(j; t)$  through the control law of (4.1). These are used to modulate the motion trajectory  $X(t), Y(t)$ , i. e. the torch velocity  $\underline{V}(t)$  and power  $Q(t)$  (Eqs. (4.3) (4.4)) every sampling period  $Dt = 1$  s, by the sampled weighted attraction guidance tique. This is applied to a total of  $N = 10$  sampled locations on the weld surface, with  $N$  selected as a compromise between heat source

agility and path smoothness. In Eqs. (4.3) and (4.4) the optimized control gains are  $C_V = 0.0078/J$ ,  $C_Q = 0.34$  and distribution radius  $s = 20$  mm. For off-line design of the control matrix  $K$  in Eq. (4.1), initial estimates of the certain matrix parts ( $A_0, B_0$ ) in the model of Eq. (3.4) are obtained by the analytical expressions of Eqs. (3.1) and (3.5), while their uncertain components  $DA(t)$ ,  $DB(t)$  in Eq. (3.6) are obtained by the numerical simulation by thermal perturbations from the nominal conditions ( $T_d, Q_d$ ). During both the computer and laboratory tests, this thermal control strategy circulates the heat source around the processed triangular pattern, so as to emulate the ideal line source by the scanning motion of the torch to the plate regions where its heat action is needed most. For the laboratory tests, Figure 4.2b shows its crooked trajectory, consisting of consecutive segments for each period  $Dt$ , lying within a triangular band surrounding the sides of the scan welded  $\Delta$  section. Figure 5.1a illustrates the experimental time response of the torch power  $Q(t)$ , before settling to an almost steady value of about 1.8 kW. Its fluctuations relate to the random deviations of the torch position on its jagged path during each period  $Dt$  from the ideal triangular pattern. The respective laboratory transients of temperatures at the three corners  $A, B, C$  of the  $\Delta$  section are shown in Figure 5.1b, together with the open-loop time response of the reference temperature of Figure 4.2a on the section edges. The noise of these experimental temperature data by the infrared pyrometer is attributed to variations of the surface emissivity value on the scan welded plate. Finally, the resulting top surface temperature hill at the process steady state (after 20 s) is illustrated in Figure 4.2b and 4.2c as measured experimentally and as computed by the numerical simulation.

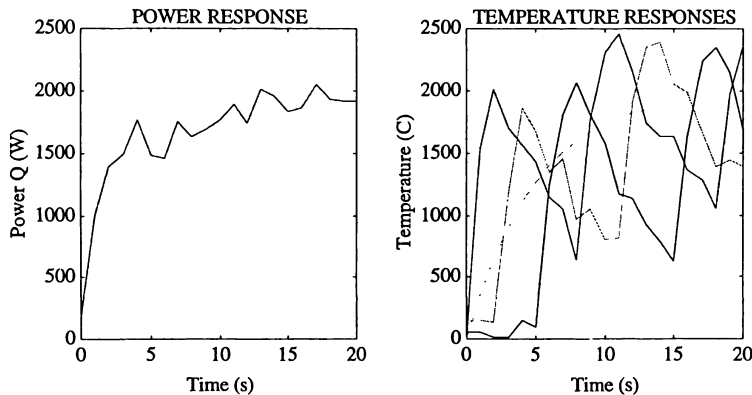


Fig. 5.1. Torch power  $Q(t)$  and corner temperature responses  $T(t)$  during closed-loop scan welding.

In Figures 4.2b and 4.2c, the clear correspondence between the measured and the computed temperature field validates the numerical simulation as a thermal model of scan welding. However, it appears that the thermal control system succeeds in generating the specified temperature distribution  $T_d$  of Figure 4.2a only partially, i.e. mainly in the vicinity of the current torch position. This is because the rest of

the previously heated region finds the time to cool down between successive passes of the torch, i.e. before the source arrives again to restore the desired thermal field. The same effect is also clearly observed at the temperature transients of Figure 5.1b, where the intermediate peaks and cooling intervals relate to the repeated passes of the torch over each corner of the triangle. This performance limitation is attributed to the slow motion of the source on its trajectory relative to the thermal dynamics of the part, because of the long torch repositioning time  $Dt = 1$  s needed to cover the time-consuming temperature measurements by the infrared camera. This problem calls for a faster thermometry transducer or parallel sensing of the thermal data in each iteration, to speed up the torch transitions. For such an assumed repositioning time  $Dt = 0.4$  s, the numerically simulated temperature field at steady state (Figure 4.2d) approaches more closely the specified reference distribution  $T_d$  of Figure 4.2a.

## 6. SUMMARY

In conclusion, the laboratory tests and computer simulations above validate the distributed-parameter sampled weighted attraction method for thermal control of the scan welding process. This heat source guidance technique adjusts the torch power and guides its motion towards the weld area of the highest actuation deficiency, by synthesizing its total intensity and velocity by partial components to a number of randomly sampled locations, weighted according to their thermal needs. This algorithm yields a dynamic trajectory tracking the moving global maximum of the required heat input distribution, to realize its optimal approximation by the heat source action. The necessary heat input is determined by a multivariable thermal control law, utilizing temperature feedback from the weld surface by an infrared camera. This controller is based on an analytical, linearized thermal conduction model of the scan welding process, expressed in state space and established on the Green's field concept. The closed-loop scan welding system is tested off-line on a flexible numerical simulation of scan welding, and in-process on a robotic GTAW setup with infrared thermometry feedback. This distributed-parameter thermal control methodology was developed so as to match the innovative redesign of a class of distributed, parallel thermal materials processing techniques, such as scan welding, and to harness the benefits of their inherent infinite-dimensional actuation and process features. In particular, the regulated temperature field and controlled thermal cycles in the scan welding application of Figures 4.2 and 5.1 yields an elongated, uniform weld pool spanning the full length of the joint centerline, and solidifying at a specified rate in progressive cross sectional increments. This contrasts to the localized ellipsoidal molten puddle in traditional sequential welding, which solidifies at the back of the mushy zone in longitudinal increments, at a rate dependent on the torch velocity. Thus, scan welding yields a better grain interweaving at the solid-melt interface, with fewer solidification defects, as well as a desirable microstructure in the heat affected zone (i.e. with limited sensitization in stainless steel welds), and minimal residual stresses and thermal distortions of the joint. The result is a demonstrated consistent increase of the tensile strength of thermally controlled scan welds

over conventional joints [4]. Besides these quality advantages, productivity features of distributed-parameter heating include process speed, efficiency and elimination or simplification of postheating and inspection requirements. However, application of the thermal control strategy above is clearly not limited to scan welding, and current research is in progress on its implementation in scan heat treatment and thermal rapid prototyping processes.

## APPENDIX A

The uncertain parts of the system matrices in Eq. 7  $DA(t)$  and  $DB(t)$  actually depend respectively on the vectors  $\underline{r}(t) \in R^p$  and  $\underline{s}(t) \in R^q$  of time-varying thermal process parameters. For example, the state matrix  $A$  is affected by the thermal diffusivity of the material  $\alpha$  and the heat transfer coefficient to the shielding gas flow  $a$ , i. e.  $\underline{r}(t) \equiv [\alpha(t) a(t)]$  ( $p = 2$ ), while the input matrix  $B$  is additionally affected by the torch efficiency  $\eta$  and distribution  $\sigma$ , i. e.  $\underline{s}(t) \equiv [\alpha(t) a(t) \eta(t) \sigma(t)]$  ( $q = 4$ ). The following conditions apply to this thermal model:

1. The constant matrices  $A_0, B_0$  constitute a controllable pair (i. e. the respective controllability matrix  $\mathcal{C}[A_0, B_0]$  is of full rank  $n$ ), because of their sparse, diagonally banded structure.
2. The uncertain matrices  $DA(\underline{r})$  and  $DB(\underline{s})$ , expressing temperature rates due to the temperature state and heat input, are continuous in the thermal parameter vectors  $\underline{r}$  and  $\underline{s}$  respectively.
3. The time-varying thermal parameters  $\underline{r}(t)$  and  $\underline{s}(t)$  reflect physical process conditions and thus are continuous functions of time and Lebesgue measurable.
4. The vectors  $\underline{r} \in \mathcal{R} \subset R^p$  and  $\underline{s} \in \mathcal{S} \subset R^q$  belong to the known, compact bounding sets  $\mathcal{R}$  and  $\mathcal{S}$  respectively, defined by the variation ranges of the respective parameters.
5. The uncertain matrices  $DA, DB$  are matched by  $B_0$ , i. e. one can determine the matrix functions:

$$\begin{aligned}
 D(\underline{r}) &= (B_0^T B_0)^{-1} B_0^T DA(\underline{r}) \quad \text{of dimension } m \times n, \text{ such that} \\
 &DA(\underline{r}) = B_0 D(\underline{r}) \quad \forall \underline{r} \in \mathcal{R} \\
 E(\underline{s}) &= (B_0^T B_0)^{-1} B_0^T DB(\underline{s}) \quad \text{of dimension } m \times m, \text{ such that} \\
 &DB(\underline{s}) = B_0 E(\underline{s}) \quad \forall \underline{s} \in \mathcal{S}
 \end{aligned} \tag{A.1}$$

Thus, the problem of robust stabilizing control of thermal processing in this MIMO-LTV formulation is posed as the design of a feedback control law  $\underline{Q} = K \times \underline{T}$  such that for all initial temperature conditions  $T_d$  and all parameter alterations  $\underline{r} \in \mathcal{R}$  and  $\underline{s} \in \mathcal{S}$ , the thermal steady state  $T$  tends to  $T_d$  of the nominal process conditions as  $t \rightarrow \infty$ . The  $m \times n$  matrix of controller gains  $K$  can be designed according to the following algorithm [4]:

- A  $m \times n$  controller gain matrix  $K_0$  is designed so that the control law  $Q = K_0 T$  places the eigenvalues of the stationary, closed-loop system matrix  $\hat{A}_0 = A_0 + B_0 K_0$  at the desired stable locations. Because of Condition 1 above, this is always possible and can be done through e.g. the Bass-Gura or Ackermann algorithms [1].
- A positive definite symmetric matrix  $J$  is selected (e.g.  $J = I_{n \times n}$ ) and the Lyapunov equation is solved for the  $n \times n$  positive definite symmetric matrix  $P$ :

$$A_2 \hat{A}_0^T P + P \hat{A}_0 = -J \quad (\text{A.2})$$

- The following matrix function is defined:

$$M(\underline{r}, \underline{s}) = -J + P B_0 [D(\underline{r}) + E(\underline{s}) K_0] + [D(\underline{r}) + E(\underline{s}) K_0]^T B_0^T P \quad (\text{A.3})$$

- A scalar  $\beta$  and a  $m \times n$  matrix  $\Omega$  are defined as:

$$\beta = \min \{ \lambda_{\min} (2I_{m \times M} + E(\underline{s}) + E^T(\underline{s})) : \underline{s} \in \mathcal{S} \} \text{ and } \Omega = \sqrt{\beta \cdot B_0 P} \quad (\text{A.4})$$

where the function  $\lambda_{\min}(N)$  denotes the minimum eigenvalue of a symmetric matrix  $N$ .

- A matrix  $P$  is constructed, the columns of which span the null space of  $\Omega$ , i.e.  $\Pi(\Omega) = [\underline{z} : \Omega \underline{z} = 0]$  and a  $n \times m$  matrix  $\Theta = P B_0$ .
- The scalar quantity  $\gamma^*$  is determined as:

$$\gamma^* = \frac{\max \{ \lambda_{\max} (\Theta^T M(\underline{r}, \underline{s}) \Theta) : \underline{r} \in \mathcal{R}, \underline{s} \in \mathcal{S} \}}{\lambda_{\min} (\Theta^T \Omega^T \Omega \Theta)} \quad (\text{A.5})$$

$$= \frac{\max \{ |\Pi^T M(\underline{r}, \underline{s}) \Theta|^2 : \underline{r} \in \mathcal{R}, \underline{s} \in \mathcal{S} \}}{\lambda_{\min} (\Theta^T \Omega^T \Omega \Theta) \cdot \max \{ \lambda_{\max} (\Pi^T M(\underline{r}, \underline{s}) \Pi) : \underline{r}, \underline{s} \in \mathcal{S} \}}$$

where the function  $\lambda_{\max}(N)$  denotes the maximum eigenvalue of a symmetric matrix  $N$ , and the norm of matrix  $N$  is defined as  $|N|^2 = \lambda_{\max}(N^T N)$ . Note also that:

$$\max \{ \lambda_{\max} (\Pi^T M(\underline{r}, \underline{s}) \Pi) : \underline{r} \in \mathcal{R}, \underline{s} \in \mathcal{S} \} = \lambda_{\max} (-\Pi^T j \Pi) = -\lambda_{\min} (\Pi^T j \Pi) \quad (\text{A.6})$$

which simplifies the calculation of  $\gamma^*$ .

- A non-negative scalar  $\gamma$  is selected, such that  $\gamma > \gamma^*$ , to construct the  $m \times n$  controller gain matrix:

$$DK = -\gamma B_0^T P. \quad (\text{A.7})$$

It follows that, under the specific Conditions 1 through 5 above, a robust linear stabilizing control law of the thermal process is given for any  $\gamma > \gamma^*$  by Eq. (4.1), i.e. for the  $m \times n$  controller gain matrix  $K = K_0 + DK$ , the closed-loop system of

Eq. (4.2) tends asymptotically to the stable equilibrium of the nominal operating point, i. e. the eigenvalues of matrix  $\hat{A}(\underline{r}, \underline{s}) = A(\underline{r}) + B(\underline{s}) \cdot K$  are guaranteed to lie in the left-half complex plane for all  $\underline{r} \in \mathcal{R}$ ,  $\underline{s} \in \mathcal{S}$ . This result is proven on the basis of the robust stabilizing control theorem for matched systems [12].

(Received April 8, 1998.)

#### REFERENCES

- 
- [1] K. J. Astrom and B. Wittenmark: Adaptive Control. Addison-Wesley, Reading 1995.
  - [2] H. S. Carslaw and J. C. Jaeger: Conduction of Heat in Solids. Oxford Press, London 1959.
  - [3] M. Delfour and S. K. Mitter: Controllability and observability for infinite dimensional systems. SIAM J. Control 10 (1972), 329-333.
  - [4] C. C. Doumanidis: Modeling and control of timeshared and scanned torch welding. ASME J. of Dynamic Systems, Measurement and Control 116 (1994), 3, 387-395.
  - [5] C. C. Doumanidis and D. E. Hardt: Simultaneous in-process control of heat-affected zone and cooling rate ruring arc welding. Welding Journal 69 (1990), 5, 186s-196s.
  - [6] I. S. Duff and D. J. Stewart: Sparse Matrix Proceedings. SIAM, Philadelphia, 1979.
  - [7] M. B. Hale and D. E. Hardt: Multi-output process dynamics in GMAW: limits to control. Internat. Trends in Welding Science and Technology, ASM Gatlinburg TN, (1992), 1015-1020.
  - [8] N. Metropolis and A. M. Rosenbluth and A. E. Teller: J. Chem. Phys. (1953), 1087-1092.
  - [9] H. Miyachi: *n*-Process Control of Root-Gap Changes During Butt Welding. Dept. of Mechanical Engineering, MIT, Cambridge, MA 1989.
  - [10] D. A. Murio: The Molification Method and the Numerical Solution of Ill-Posed Problems. Wiley, New York 1993.
  - [11] W. H. Ray and D. G. Lainiotis: DPS-Identification, Estimation and Control. M. Dekker, New York 1978.
  - [12] W. E. Schmitendorf and B. R. Barmish: Guaranteed asymptotic stability for systems with constant disturbances. In: Proceedings of ACC, Boston 1985.

*Charalabos C. Doumanidis, Anderson Hall, Room 221. U. S. A.  
e-mail: cdoumani@tufts.edu*